



HAL
open science

Three-dimensional numerical and analytical study of horizontal group of square anchor plates in sand

Hicham Mokhbi, Mekki Mellas, Abdelhak Mabrouki, Jean-Michel Pereira

► To cite this version:

Hicham Mokhbi, Mekki Mellas, Abdelhak Mabrouki, Jean-Michel Pereira. Three-dimensional numerical and analytical study of horizontal group of square anchor plates in sand. *Acta Geotechnica*, 2018, 13 (1), pp.159-174. 10.1007/s11440-017-0557-x . hal-02882390

HAL Id: hal-02882390

<https://enpc.hal.science/hal-02882390>

Submitted on 26 Jun 2020

HAL is a multi-disciplinary open access archive for the deposit and dissemination of scientific research documents, whether they are published or not. The documents may come from teaching and research institutions in France or abroad, or from public or private research centers.

L'archive ouverte pluridisciplinaire **HAL**, est destinée au dépôt et à la diffusion de documents scientifiques de niveau recherche, publiés ou non, émanant des établissements d'enseignement et de recherche français ou étrangers, des laboratoires publics ou privés.

Three-dimensional numerical and analytical study of horizontal group of square anchor plates in sand

Hicham Mokhbi¹, Mekki Mellas¹, Abdelhak Mabrouki¹, Jean-Michel Pereira²

¹ Civil Engineering Research Laboratory, University of Biskra, BP145 Biskra 07000, Algeria

² Laboratoire NAVIER, École des Ponts Paris Tech, 6 et 8 avenue Blaise Pascal, 77420 Champs-sur-Marne, France

Abstract

In this paper, numerical and analytical methods are used to evaluate the ultimate pullout capacity of a group of square anchor plates in row or square configurations, installed horizontally in dense sand. The elasto-plastic numerical study of square anchor plates is carried out using three-dimensional finite-element analysis. The soil is modeled by an elasto-plastic model with a Mohr-Coulomb yield criterion. An analytical method based on a simplified three-dimensional failure mechanism is developed in this study. The interference effect is evaluated by group efficiency η , defined as the ratio of the ultimate pullout capacity of group of N anchor plates to that of a single isolated plate multiplied by number of plates. The variation of the group efficiency η was computed with respect to change in the spacing between plates. Results of the analyses show that the spacing between the plates, the internal friction angle of soil and the installation depth are the most important parameters influencing the group efficiency. New equations are developed in this study to evaluate the group efficiency of square anchor plates embedded horizontally in sand at shallow depth ($H=4B$). The results obtained by numerical and analytical solutions are in excellent agreement.

Keywords

Square anchor plate, group efficiency, finite elements, pullout capacity, sand, critical spacing.

27 1 Introduction

28 Anchor plates are lightweight structural elements, buried in the ground, used to resist
29 the pullout forces acting on geotechnical structures such as submerged pipelines,
30 offshore structures, retaining walls, and transmission towers. They may have various
31 shapes (circular, helical, square, rectangular or strip). They are installed in the
32 ground horizontally, vertically or in an inclined way. In the literature there are different
33 theoretical, numerical and experimental works investigating the behavior of an
34 isolated anchor plate and calculate its ultimate uplift capacity. One can cite Meyerhof
35 and Adams (1968), Das (1978), Murray and Geddes (1987), Merifield and Sloan
36 (2006), Hanna et al (2007), Khatri and Kumar (2009, 2010, 2011), Wang et al (2013),
37 Bhattacharya and Kumar (2014), Mabrouki and Mellas (2014), Ardebili et al (2016),
38 among others.

39 However, little information is available in the literature concerning the ultimate pullout
40 capacity of a group of anchor plates. Table 1 presents some experimental, analytical
41 and numerical works. Meyerhof and Adams (1968) proposed a theoretical
42 relationship for calculating the ultimate pullout force of group of circular or rectangular
43 foundations, buried in sand or in clay. Das and Yang (1987) have developed a
44 physical model to evaluate the ultimate pullout force of a group of circular anchor
45 plates buried in medium dense sand. They compared their results in terms of group
46 efficiency with the theoretical solution of Meyerhof and Adams (1968), and they found
47 that the ratio spacing/diameter (S/D) for a group efficiency $\eta = 100\%$, for a given
48 configuration, is approximately equal to the double of the one obtained theoretically.
49 However, the general trend of the evolution of the group efficiency with respect to
50 S/D ratio is similar to that of the theory.

51 In the present study, special attention was paid to the experimental model of Geddes
52 and Murray (1996), to study the pullout force of a group of square anchor plates

53 embedded in a dense sand at a fixed depth, in different configurations. They reported
54 that, from a critical spacing ratio ($S_{cr}/B = 2.9$ for the test conditions used), the
55 maximum group efficiency is 100% and remains at that level when increasing the
56 spacing. This critical spacing is valid for all configurations and for a number of studied
57 anchor plates.

58 Abbad et al. (2013), have carried out an experimental study of the interaction of the
59 failure zones of square anchor plates installed at a depth of $5B$ in an analogical
60 environment formed by plastic granules. They used digital photographs at high
61 resolution processed by image correlation software to observe the displacement field
62 and plane strain of the analogical environment. They have reported that a minimum
63 spacing between axes of about seven times the width of the plate ($7B$) is necessary
64 for two neighboring anchor plates to act independently of each other.

65 In addition, other analytical studies of interferences within a group of strip anchor
66 plates, were established by Kumar and Kouzer (2008a), Kouzer and Kumar (2009a,
67 2009b), Merifield and Smith (2010), Ghosh and Kumari (2012), Kumar and Naskar
68 (2012), and Sahoo and Kumar (2014a, 2014b). These works fall within the limit
69 analysis framework, using the lower bound or the upper bound method. Table 1
70 shows the previous experimental and analytical works related to the study of the
71 interference of anchor plates in soils.

72 The main objective of this study is, on the one hand, to investigate numerically, using
73 three-dimensional non-linear finite element analysis, the group efficiency of square
74 anchor plates buried horizontally in a dense sand for several values of spacing/width
75 ratio (S/B). The effect of parameters like installation depth, internal friction angle of
76 soil, anchor roughness, and flow rule have been investigated numerically. On the
77 other hand, an additional objective is to develop an analytical solution of the group
78 efficiency of square anchor plates buried horizontally in the sand based on a failure

79 mechanism available in the literature, where a modification of the shape of the failure
80 mechanism was introduced to simplify the calculation of the interference of failure
81 mechanisms.

82 This study aims at highlighting recommendations concerning the calculation of pullout
83 capacity of group of square anchor plates buried horizontally in a dense sand.

84 **2 Numerical modeling**

85 In this study, a three-dimensional numerical model was developed using the finite
86 element method in Plaxis software, to investigate the ultimate uplift capacity of a
87 group of square plate anchors. From previous experimental and theoretical studies
88 on groups of plate anchors in soil (Table 1), the experimental work of Geddes and
89 Murray (1996) seems the most appropriate as a reference for our work because it
90 concerns the problem of square plates and contains the required data for numerical
91 modeling. Geddes and Murray (1996) have performed a series of laboratory pullout
92 tests on group of square plate anchors buried horizontally in dense sand. These tests
93 were conducted in a steel box of size $1.28m \times 1.22m \times 0.89m$. The plate anchor
94 have a square shape of width $B = 50.8mm$, buried at a fixed depth $H = 203.2mm$ to
95 give a ratio $H/B = 4$. Vertical uplift tests were carried out on two and five square
96 plates in row configuration with constant spacing; and on groups of four square
97 plates placed in a square configuration.

98 The symmetry of the problem enables to take a quarter model in all calculations as
99 shown in Fig.1 which presents an example of a group of four anchor plates in square
100 configuration. The dimensions of the numerical model adopted in all calculations
101 (width, length and height) are constants according to the experimental model of
102 Geddes and Murray (1996). The width of the model adopted is $0.61m$ and the height
103 is $1m$; the square plate anchor have a width of $B = 50mm$. It is verified that these

104 dimensions do not prevent the development of the failure mechanism for the large
105 values of the spacing (S) considered in this study.

106 The small displacement assumption has been considered in all numerical analysis.
107 The adopted soil model is a linear elastic-perfectly plastic model, obeying Mohr–
108 Coulomb criterion with a non-associative flow rule. Referring to the study of Bolton
109 (1986) on the strength and dilatancy of sands, the adopted dilation angle is $\psi' = \phi' -$
110 30° . The anchor plate is modeled by plate elements with a linear elastic model. The
111 values of soil parameters and elastic stiffness parameters of plate anchor used in this
112 investigation are shown in Table 2. The soil parameters were taken from the Geddes
113 and Murray (1996) study, and the elastic parameters of the material constituting the
114 anchor plates were estimated from the literature studies (e.g., Hanna et al, 2011,
115 Aghazadeh Ardebili et al, 2015, Ghosh, and Kumari, 2012).

116 Interface elements are used between soil and anchor plate elements to ensure soil-
117 plate interaction. This type of interface elements allow for soil detachment. The
118 interface behavior is defined by Mohr Coulomb criterion, with shear-strength
119 characteristics calculated by the introduction of the strength reduction factor $R_{inter} \leq$
120 1 , which gives the values of strength parameters of the interface element from the
121 soil parameters by applying the strength reduction method suggested by Plaxis
122 (Brinkgreve and Vermeer 2001) as follows:

$$123 \quad c'_i = R_{inter} c'_{soil},$$

$$124 \quad \tan \varphi'_i = R_{inter} \tan \varphi'_{soil} \leq \tan \varphi'_{soil}$$

$$125 \quad \psi'_i = 0^\circ \text{ for } R_{inter} < 1, \text{ otherwise } \psi'_i = \psi'_{soil}$$

126 where c'_i , φ'_i and ψ'_i are the cohesion, the friction angle and the dilation angle of
127 interface elements respectively.

128 A modified shear box test carried out by Geddes and Murray (1996) gave an
129 interface friction angle of 10.6° for the sand studied in contact with polished steel
130 plates, of the same kind as the anchors plates used in the uplift test. So for our case
131 the strength reduction factor $R_{inter} = 0.19$.

132 Prescribed upwards displacements were applied at the nodes of anchor plates, and
133 increase gradually until the stabilization of the resultant force which corresponds to
134 the ultimate pullout force Q_u of the anchor plates group (Fig. 5). It should be noted
135 that, using a displacement loading procedure, the parameters of the plate anchor do
136 not affect the calculation results.

137 Before adopting the reference numerical model, several calculation tests were
138 executed to check the influence of the mesh and the size of the model on calculation
139 results, which allowed to suggest not only the use of a fine mesh in the vicinity of the
140 anchor plate but also that the plate element itself must imperatively be discretized in
141 10 elements minimum on the x-y plane to get more accurate results. It was also
142 verified that the boundaries of the numerical model based on the dimensions of the
143 experimental model of Geddes and Murray (1996) have no effect on the value of the
144 ultimate force obtained. It was finally checked that the values of the elastic
145 parameters of soil have a negligible effect on the ultimate force computed by the
146 numerical analysis.

147 **3 Numerical results**

148 The numerical finite element analyses that have been performed in this study
149 concern the calculation of the ultimate pullout capacity of a group of square anchor
150 plates, installed in row configuration: two (2×1), three (3×1), four (4×1) and five (5
151 $\times 1$) square plates, or in square configuration: four (2×2) and nine (3×3) square
152 plates, with a constant spacing S between the plates varying between 0 and $2.5B$.

153 The group efficiency η was analyzed as a function of the spacing/width ratio (S/B) for
154 both row and square configurations for these relatively low values of S/B ratio. Then
155 the critical spacing S_{cr} between anchor plates was evaluated (corresponding to $\eta =$
156 100%). S_{cr} was defined as the distance from which each anchor plate acts
157 independently without interference between failure mechanisms (results discussed in
158 section 6).

159 **3. 1 Group of square anchor plates in row configuration**

160 Before starting the numerical analyses for group of plates, the pullout capacity of an
161 isolated square anchor plate was calculated. The evolution of pullout load with
162 displacement was plotted in Fig. 5 (bottom curve). The failure mechanism of this
163 isolated square anchor plate can be observed in Fig. 2. Its shape can be considered
164 as a truncated cone with slightly curved failure planes near the ground surface.

165 In order to investigate the influence of elastic parameters of soil on the ultimate
166 pullout capacity, the case of a single square anchor plate are analysed with different
167 values of Young's modulus ($E = 10, 30$ and 60 MPa). Fig. 3 shows the results
168 obtained for $H/B = 4$ and $H/B = 6$; It can be observed that the values of the elastic
169 parameters have a small effect on the ultimate pullout capacity. However, for great
170 values of E the ultimate load is reached for a smaller displacement.

171 Fig. 4 illustrates a group of square anchor plates of width B , installed in row
172 configuration with a similar spacing S . The total line length is noted L .

173 Fig. 5 shows the results of the ultimate pullout load as a function of displacement for
174 a group of two square anchor plates with different values of S/B ratio varying from 0
175 to 2, indicating that the force Q_u increases with increasing spacing between the two
176 anchor plates. This trend illustrates the presence of group effects on the ultimate
177 pullout capacity. Fig. 6 presents the total displacements obtained in the case of two

178 anchor plates with a ratio of $S/B = 2$. It also shows the interference of the failure
179 mechanisms of the two adjacent plates.

180 The group efficiency η was calculated by the following conventional relation (Das
181 (1990), Geddes and Murray (1996), Emirler et al (2015)):

$$\eta (\%) = \frac{\text{Ultimate load of group of } N \text{ anchors} \times 100}{N \times \text{ultimate load of an isolated anchor}} \quad (1)$$

182 with N the total number of anchor plates.

183 Fig. 7 shows the evolution of the group efficiency of square anchor plates in row
184 configuration (two (2×1), three (3×1), four (4×1) and five (5×1)) with the
185 spacing/width ratio (S/B). In the same figure are plotted the experimental results
186 obtained by Geddes and Murray (1996) in the case of two (2×1) and five (5×1)
187 plates.

188 The numerical results show that the evolution of the group efficiency as a function of
189 (S/B) ratio is perfectly linear, and may be fitted with Equations (2), (3), (4) and (5) for
190 configurations (2×1), (3×1), (4×1) and (5×1) respectively. For the case of two plates
191 (2×1), the group efficiency η increases linearly from 61% for $S/B = 0$ corresponding
192 to a rectangular plate $L/B = 2$ to 78% for $S/B = 2$. For the case of three plates (3×1),
193 η increase linearly from 48% for $S/B = 0$ corresponding to a rectangular plate $L/B = 3$
194 to 77% for $S/B = 2.5$. For the case of four plates (4×1), η increase linearly from 41%
195 for $S/B = 0$ corresponding to a rectangular plate $L/B = 4$ to 74% for $S/B = 2.5$. For five
196 plates (5×1), η increase also linearly from 37% for $S/B = 0$ corresponding to a
197 rectangular plate $L/B=5$ to 72% for $S/B = 2.5$.

$$\eta_{2 \times 1}(\%) = 8.537 \frac{S}{B} + 60.96 \quad (2)$$

$$\eta_{3 \times 1}(\%) = 11.45 \frac{S}{B} + 48.13 \quad (3)$$

$$\eta_{4 \times 1}(\%) = 13.25 \frac{S}{B} + 40.68 \quad (4)$$

$$\eta_{5 \times 1}(\%) = 13.85 \frac{S}{B} + 36.94 \quad (5)$$

198 The values of group efficiency obtained experimentally by Geddes and Murray (1996)
 199 are larger than the numerical results, except for the first point ($S/B = 0$) which is
 200 superimposed to the numerical point in both cases (2×1) and (5×1). For the case of
 201 five plates (5×1), the difference between the experimental and numerical results
 202 increases with the increase of S/B ratio, and remains nearly constant around 10% for
 203 the case of two plates (2×1). However, the experimental results also show a linear
 204 trend from the second point corresponding to $S/B = 0.25$ or $S/B = 0.5$. On this point,
 205 Geddes and Murray (1996) reported that the relationship between S/B and the group
 206 efficiency demonstrates an initial perturbation followed by a linear trend.

207 The group efficiency obtained experimentally varies from about 59% for $S/B = 0$ to
 208 about 90% for $S/B = 2$ in the case of two plates (2×1). For five plates, η varies from
 209 about 37% for $S/B = 0$ to about 71% for $S/B = 2.5$.

210 From these results in row configuration, we can conclude that the group efficiency of
 211 N plates is lower than that of $(N - 1)$ plates for the same spacing S , and this
 212 difference of efficiency decreases when the spacing/width ratio (S/B) increases.

213 **3. 2 Group efficiency of square plates in square configuration**

214 For a square configuration, Fig. 8 illustrates the two cases studied: groups of four (2
 215 $\times 2$) and nine (3×3) square anchor plates. Fig. 9 presents the total displacements
 216 obtained in the case of nine anchor plates with a ratio of $S/B = 2$. It also shows the
 217 interference between failure mechanisms of plates.

218 Fig. 10 shows the numerical results of these cases in comparison with the
 219 experimental results obtained by Geddes and Murray (1996). The numerical results

220 show that η increases linearly as a function of S/B ratio, following the two Equations
221 (6) and (7) for the case of four (2×2) and nine (3×3) plates respectively. For the
222 case of four plates (2×2), η evolves linearly from 34% for $S = 0$ (corresponding to a
223 single square plate of width equal to $2B$), to 67% for $S/B = 2.5$. For the case of nine
224 (3×3) plates, η increase from 20% for $S = 0$ (corresponding to the case of a single
225 square plate of width equal to $3B$), to 52% for $S/B = 2.5$.

226 The experimental results of Geddes and Murray (1996) for four square plates (2×2),
227 shows that η evolves almost linearly with S/B ratio, from 34% for $S = 0$ to
228 approximately 85% for $S/B = 2.5$. However, the experimental values of η are larger
229 than the numerical values except for the case of $S/B = 0$ where the values of η are
230 equal, then the difference between the numerical and experimental values of η
231 increases gradually with the increase of S/B .

$$\eta_{2 \times 2}(\%) = 13.39 \frac{S}{B} + 33.48 \quad (6)$$

$$\eta_{3 \times 3}(\%) = 12.92 \frac{S}{B} + 19.81 \quad (7)$$

232 It is also remarkable that for any given value for S/B ratio, the group efficiency of four
233 square anchor plates installed in square configuration is lower than in the case of
234 four square anchor plates installed in row configuration. The reason is that in square
235 configuration, the failure mechanism of each of the four plates interferes with that of
236 the two or three other plates. In row configuration, the failure mechanism of each of
237 the intermediate plates interferes with that of the two nearby plates, and the failure
238 mechanism of each of the edge plates interferes only with that of a single plate. This
239 difference of group efficiency between a row and square configuration becomes
240 larger with the increase of the number of anchor plates.

241 3.3 Load factors

242 The previous numerical results highlighted that the group efficiency of a group of
243 square anchor plates installed horizontally in sand, in row or square configuration,
244 evolves linearly with S/B ratio. In order to establish a general equation of the group
245 efficiency of N anchor plates, the previous data of group efficiency, for row and
246 square configurations, were redrawn in terms of load factor F_L versus L/B ratio.
247 According to Geddes and Murray (1996), the following relationship holds:

$$\frac{L}{B} = n + (n - 1) \frac{S}{B} \quad (8)$$

248 with n the number of plate per row,

$$F_L = \frac{\textit{Ultimate load of } N \textit{ plates}}{\textit{Ultimate load of a single isolated plate}} \quad (9)$$

249 or

$$F_L = \eta \times N/100 \quad (10)$$

250 Fig. 11 presents the variation of the load factor according to L/B ratio for all row
251 configurations studied previously. The load factor evolves linearly with L/B ratio for
252 two, three, four and five anchor plates in row configuration. This linear relation is best
253 fitted by the following equation:

$$F_L = 0.182 (L/B) + 0.866 \quad (11)$$

254 From Equations (8), (10) and (11), we can write a general relation (12) of the group
255 efficiency of n square anchor plates installed horizontally in the sand in row
256 configuration ($n = N$). Nevertheless, this relation is valid only for the geotechnical and
257 geometrical characteristics chosen in this study.

$$\eta_{n \times 1}(\%) = \frac{18.2}{n} \left(n + (n - 1) \frac{S}{B} \right) + \frac{86.6}{n} \quad (12)$$

258 Besides, by drawing the curve of the load factor according to L/B ratio for the case of
 259 four and nine anchor plates in square configuration (Fig. 12), a global linear relation
 260 of the evolution of the load factor is obtained:

$$F_L = 0.561 (L/B) + 0.167 \quad (13)$$

261 So, from equations (8), (10), and (13) we can write the general relation (14) of the
 262 group efficiency of ($N = n \times n$) square anchor plates installed horizontally in the sand
 263 in square configuration, which also is valid only for the geotechnical and geometrical
 264 characteristics considered in this study:

$$\eta_{n \times n}(\%) = \frac{56.1}{n^2} \left(n + (n - 1) \frac{S}{B} \right) + \frac{16.7}{n^2} \quad (14)$$

265 **4 Parametric study**

266 The previous numerical calculations have established the general Equations (12) and
 267 (14) of the group efficiency for row and square configurations respectively. These
 268 relations concern the case of $H/B = 4$, and involve the following variables: number of
 269 anchor plates, spacing between anchor plates and width of plates. However, a
 270 parametric study is needed to verify the influence of various parameters on the
 271 obtained results. To this aim, a numerical parametric study was carried out on a
 272 group of two square anchor plates, studying the influence of installation depth,
 273 internal friction angle of soil, flow rule and roughness of anchors.

274 **4.1 Influence of installation depth**

275 To study the influence of installation depth on the group efficiency, the ultimate
 276 pullout capacity of two square anchor plates was calculated for a depth/width ratio

277 $H/B = 2$ and $H/B = 6$. Then the group efficiency was calculated and compared with
278 those obtained for the reference model ($H/B = 4$) as shown in Fig. 13.

279 Fig. 13 shows that the group efficiency for a given spacing decreases when the H/B
280 ratio increases. Indeed, the critical spacing (S_{cr}) increases with depth (H). This is
281 explained by the relationship between the critical spacing and the installation depth
282 theoretically estimated by $S_{cr} = 2H \tan \theta$, with θ is the inclination angle of the failure
283 plane with the vertical as shown in Fig. 21.

284 In previous studies, the installation depth has also an influence on the shape of
285 failure mechanisms. There is a critical embedment ratio which presents the transition
286 between shallow anchor behaviour and deep anchor behaviour. Meyerhof (1973)
287 proposed a critical embedment ratio $H/B = 4$ for square anchors in loose sand, and it
288 increases up to about 8 in dense sand. Also, Das (1983) proposed an empirical
289 correlation for the critical embedment ratio for square anchor plates in the form
290 $H/B = 5.5 + 0.166(\varphi - 30)$, (for $30^\circ \leq \varphi \leq 45^\circ$).

291 Fig. 14 shows the total displacement for the case of two square anchor plates
292 embedded at different depths with H/B varying from 4 to 10. The mechanisms are
293 depicted by the contours of finite element displacement; where the same scale was
294 used to present the displacement field for all embedment ratio values. It is seen that
295 from embedment ratio $H/B \geq 8$ the failure mechanism begins to develop locally.
296 From the present study, the embedment ratio $H/B = 8$ can be considered as the
297 critical embedment ratio.

298 **4.2 Influence of internal friction angle**

299 The reference numerical model was studied with an internal friction angle $\varphi' = 43.6^\circ$.
300 However, to study the influence of this parameter on the group efficiency, other
301 numerical calculations were performed, also for a group of two square anchor plates,

302 with other values of the internal angle friction $\varphi' = 30^\circ$ and $\varphi' = 20^\circ$. For these values
303 of φ' , the adopted dilation angle is equal to zero. The results of numerical calculations
304 are presented in Fig. 15 showing a little influence compared to the depth parameter
305 on the group efficiency. η increases by 8% when φ' decreases from 43.6° to 20° . This
306 influence can be explained by the relation of the failure mechanism with the internal
307 friction angle. Some authors such as Clemence and Veesaert (1977) found that the
308 inclination angle of the failure plane with the vertical is equal to the half of the internal
309 friction angle of soil. Murray and Geddes (1987), and Merifield et al (2006) found that
310 this inclination angle is equal to the internal friction angle. So, when φ' decreases the
311 interference between failure mechanisms decreases and η increases.

312 **4.3 Influence of dilation angle**

313 To study the influence of the flow rule on the group efficiency, other numerical
314 calculations were established for the case of two square anchor plates. An
315 associated flow rule ($\psi' = \varphi'$) was considered, and the obtained results of the group
316 efficiency were compared with the results of the reference case calculated with a
317 non-associated flow rule ($\psi' = \varphi' - 30^\circ$). This comparison is presented in Fig. 16 and
318 shows an almost negligible effect on the group efficiency according to S/B ratio.
319 However, it should be noted that there is a significant influence of the dilation angle
320 on the value of the ultimate pullout capacity, which is overestimated with an
321 associated flow rule (up to 38%).

322 **4.4 Influence of anchor roughness**

323 In the reference model, the interface between the soil and the anchor plate was
324 determined by using a strength reduction factor $R_{inter} = 0.19$. To study the influence
325 of anchor roughness on the group efficiency, other calculations were performed for a
326 group of two square anchor plates, with the following values of the strength reduction

327 factor $R_{inter} = 0.33; 0.5; 0.75$ and 1. The results of group efficiency are presented in
328 Fig. 17, which show that there is a very little influence on the values of group
329 efficiency. This is can be explained by the shape of failure mechanism, where there is
330 no significant mobilization of shearing resistance between the soil and the anchor
331 plate during the pullout action. Rowe and Davis (1982b) found that the roughness
332 has a negligible effect on the capacity of horizontal anchors at all depths, but
333 significantly increases that of shallow vertical anchors ($H/B < 3$). For this latter case,
334 they found that the effect of roughness is increased further if the soil is dilatant.

335 **5 Analytical solution for n square anchor plates in row configuration**

336 **5.1 Isolated anchor plate**

337 Murray and Geddes (1987) have developed a failure mechanism using the upper
338 bound limit analysis, for a rectangular anchor plate installed horizontally in a frictional
339 soil, and subjected to a vertical pullout loading. This failure mechanism consists in a
340 failure plane inclined at an angle φ' to the vertical at the edge of the plate. At the
341 corners the failure mechanism consists in a portion of a circular cone. They have
342 obtained the following expression for the break-out factor N_y :

$$N_y = 1 + \frac{H}{B} \tan \varphi' \left(1 + \frac{B}{L} + \frac{\pi H}{3 L} \tan \varphi' \right) \quad (15)$$

343 To simplify the analytical calculation of the interference of a group of square anchor
344 plates, the portion of a circular cone at the corners were replaced by a vertical
345 pyramid. The inclination angle (θ) of the failure plane with the vertical was adopted
346 using this empirical relation $\theta = 0.785 \varphi'^{1.1}$ with φ' is expressed in degree (Fig. 18).

347 Following the theory of Mors (1959), the ultimate pullout capacity is assumed equal to
348 the weight of soil located within the failure mechanism; and the frictional resistance
349 acting along the failure surface was ignored. Ilamparuthi et al. (2002) have reported

350 that the method of Mors (1959) is usually conservative for shallow anchors but
351 overpredicts pullout capacity for deeper anchors. This method was also followed by
352 Ganesh and Sahoo (2015) to estimate the ultimate uplift resistance of circular anchor
353 plate. They reported that the frictional resistance acting along the failure surface can
354 be ignored, conservatively, for the case of shallow anchors. It is worthwhile noting
355 that the present study considers the anchor plates embedded at shallow depth
356 ($H=4B$).

357 The break-out factor of this modified failure mechanism is given in equation (16) (see
358 details in appendix A). The values of N_γ obtained by this expression (16) give a very
359 satisfactory agreement with the upper bound results obtained by Murray and Geddes
360 (1987), and the lower bound results obtained by Merifield et al. (2006) as shown in
361 Fig. 19.

$$N_{\gamma \text{ isolated}} = 1 + 2 \frac{H}{B} \tan \theta + \frac{2}{3} \left(\frac{H}{B} \right)^2 \tan^2 \theta \quad (16)$$

362 In order to examine the effect of soil strength along the failure surface on the ultimate
363 pullout capacity, numerical analyses were carried out by modeling a full-scale square
364 plate ($B = 1\text{m}$) with embedment ratio H/B varying from 1 to 5, and $\phi' = 20^\circ, 30^\circ$ and
365 40° by considering an associative flow rule. The model adopted in these numerical
366 analyses, has a depth of 10 m and extends 6 m beyond the planes of symmetry.

367 The values of the break-out factor N_γ obtained from the present numerical analyses
368 were compared with those calculated with the expression (16) as shown in Fig. 20.

369 The comparison shows that the values of N_γ obtained by the expression (16) are
370 slightly smaller than the numerical values. Consequently, when the soil strength
371 along the failure surface is ignored, the result always errs on the safe side; it
372 underestimates the ultimate pullout capacity. However, the relative error from the use

373 of this assumption varies between 3% and 17%, and it increases slightly with the
 374 increase in embedment ratio.

375 **5.2 Two square anchor plates**

376 For a group of two square anchor plates spaced by $S < 2H \tan \theta$, the ultimate pullout
 377 capacity of each anchor plate is simply equal to the weight of the soil located within
 378 the failure mechanism (defined by points a, b, c, d, e for the left anchor, as shown in
 379 Fig. 21). The break-out factor corresponding to this volume is noted by $N_{\gamma end}$ and
 380 given by: (see details in appendix B)

$$N_{\gamma end} = 1 + \frac{1}{3} \left(\frac{H}{B} \right)^2 (\tan \theta)^2 + \frac{1}{2} \left(3 + \frac{S}{B} \right) \frac{H}{B} \tan \theta + \frac{1}{8} \frac{S}{H} \frac{S}{B} \left(\frac{1}{3} \frac{S}{B} - 1 \right) \cot \theta - \frac{1}{4} \left(\frac{S}{B} \right)^2 + \frac{1}{2} \frac{S}{B} \quad (17)$$

381 The group efficiency of two anchor plates noted $\eta_{2 \times 1}$ can be calculated with the
 382 following relationship:

$$\eta_{2 \times 1} (\%) = \frac{N_{\gamma end}}{N_{\gamma isolated}} \times 100 \quad (18)$$

383 Fig. 22 shows the group efficiency of two anchor plates as a function of S/B ratio, as
 384 predict by Equation (18), in comparison with our numerical results and the
 385 experimental results obtained by Geddes and Murray (1996). Additional calculations
 386 were performed using Plaxis software for ($S/B = 4.5, 5$ and 5.5).

387 In general, it can be noted that the analytical results are in good agreement with
 388 numerical results. However, the experimental results obtained by Geddes and Murray
 389 (1996) show higher values than both analytical and numerical results.

390 **5.3 n square anchor plates in row configuration**

391 For a group of n square anchor plates spaced by $S < 2H \tan \theta$, the ultimate pullout
 392 capacity of an intermediate anchor plate is simply equal to the weight of the soil
 393 located within the failure mechanism defined by points a, b, c, d, e, f as shown in Fig.

394 23. The break-out factor corresponding to this volume is noted $N_{\gamma inter}$ and given by:
 395 (see details in appendix C)

$$N_{\gamma inter} = 1 + \left(1 + \frac{S}{B}\right) \frac{H}{B} \tan \theta - \frac{1}{3} \frac{S}{B} \frac{S}{H} \left(\frac{1}{4} \frac{S}{B} - 1\right) \cot \theta - \frac{1}{2} \left(\frac{S}{B}\right)^2 + \frac{S}{B} \quad (19)$$

396 In this case, the group efficiency of n anchor plates can be calculated with the
 397 following expression:

$$\eta_{n \times 1}(\%) = \frac{(n - 2)N_{\gamma inter} + 2N_{\gamma end}}{n N_{\gamma isolated}} \times 100 \quad (20)$$

398 Fig. 24 shows the comparison of numerical, analytical and experimental results of the
 399 group efficiency of five square anchor plates in row configuration. These results
 400 correspond to small values of the spacing between the plates ($0 < S/B < 2$). A good
 401 agreement is observed between the analytical results and the numerical results.

402 **6 Critical spacing for two square anchor plates**

403 Based on previous analytical and numerical results, we can determine the critical
 404 spacing for which two anchor plates (placed at a depth $H = 4B$ in this study) act
 405 independently, so that the group efficiency is equal to 100%.

406 The numerical results highlight that a critical spacing of $S_{cr} = 5.5B$, is necessary for a
 407 group of anchor plates installed in linear configuration to obtain a group efficiency of
 408 100%. The critical spacing obtained by equation (12) is $S_{cr} = 4.24B$. However, the
 409 additional calculations performed for verification by Plaxis software have given a
 410 group efficiency $\eta = 97\%$ for $S/B = 4.24$ as shown in Fig. 22.

411 The analytical calculation have given results very similar to the numerical results
 412 especially for small values of S/B ($0 < S/B < 2$). However the critical spacing obtained
 413 analytically for $\eta = 100\%$ is $S_{cr} = 7.5B$ as shown in Fig. 22. Despite this remarkable
 414 difference between the critical spacing obtained by the numerical calculation and that
 415 obtained by an analytical solution, the relative error between them is of the order of

416 3.86% for a critical spacing $S_{cr} = 5.5B$. On the other hand, Geddes and Murray
417 (1996) found in their experimental study a critical spacing of $S_{cr} = 2.9B$.

418 In addition, there is little information in the literature on the critical spacing with the
419 exception of the works presented in Table 3. It is important to examine the
420 experimental study of Abbad et al. (2013) on the interference of square anchor plates
421 ($B = 5$ cm) installed at a depth of $H = 5B$ in a material made of plastic grains with a
422 diameter of 1 mm. The analogical medium has a relative density of $Dr = 96\%$ ($e_{min} =$
423 0.302 , $e_{max} = 0.855$), with a dry unit weight of $\gamma_d = 14,6$ kN/m³, a null cohesion and an
424 initial friction angle $\varphi = 39^\circ$. Using high resolution digital pictures, they have found
425 that a minimum spacing $S_{cr} = 6B$, is necessary for two anchor plates to act
426 independently.

427 Das and Yang (1987) has developed an experimental study for circular anchor plates
428 embedded in a sand with $\varphi' = 37^\circ$, he found a critical spacing $S_{cr} = 3D$. For the same
429 characteristics, Meyerhof and Adams (1986) found $S_{cr} = 1.8D$.

430 The difference observed between the critical spacing obtained numerically and that
431 obtained analytically is attributed to the shape of the failure mechanism. Analytical
432 calculations consider an associated soil ($\psi' = \varphi$), which overestimates the ultimate
433 pullout capacity and provides a larger failure mechanism, thus requiring a bigger
434 critical spacing. Inversely, the numerical calculations, account for a non-associated
435 flow rule ($\psi' = \varphi' - 30^\circ$) which induce a narrower failure mechanism thus requiring a
436 smaller critical spacing.

437 **7 Conclusion**

438 The ultimate pullout capacity of a group of square anchor plates in row or square
439 configurations was calculated, using three-dimensional finite elements analyses. The
440 square anchor plates were installed horizontally in dense sand and pulled vertically.
441 The soil is characterized by the Mohr-Coulomb yield criterion and non-associative

442 flow rule. In this study, a simple three-dimensional failure mechanism has been
443 proposed to evaluate the anchor break-out factor and the group efficiency. The
444 evolution of the group efficiency η with the spacing/width ratio (S/B) was analyzed
445 and compared with results available in the literature.

446 In this paper, a numerical parametric study was conducted on a group of two square
447 anchor plates to identify the most influential parameters on the group efficiency. This
448 parametric study revealed that the group efficiency η increases considerably with the
449 decrease of the internal friction angle ϕ' , and the installation depth H . On the other
450 hand, η is slightly influenced by the anchor roughness and the choice of an
451 associative flow rule. Nevertheless, it is worthwhile noting that the associative flow
452 rule highly overestimates the value of the ultimate pullout capacity. The group
453 efficiency of N square anchor plates installed in row configuration is greater than that
454 of N square anchor plates installed in square configuration.

455 The comparison of the numerical results with analytical solutions confirmed that the
456 proposed failure mechanism predict a group efficiency values in good agreement with
457 those obtained by elasto-plastic analyses. New equations are developed in this study
458 to evaluate the group efficiency of shallow square anchor plates ($H=4B$). The group
459 efficiency evolves linearly with S/B ratio, until a critical value of the spacing between
460 plates beyond which the anchor plates act independently. For this critical spacing, the
461 ultimate pullout load of the group arrives at its maximal value and remains stable, in
462 spite of the increase of the spacing. The value of critical spacing for which the two
463 square anchor plates can be assumed isolated, as predicted by the present
464 numerical computations, is approximately 5.5 times the width of the plate B .

465

466

467 **References**

- 468 1. Abbad, H., Meghachou, M., Dekar, C., and Daoud, S. M. (2013). Interaction of
469 Rupture Zones of Adjacent Anchor Plates in an Analogical Medium. *ETASR -*
470 *Engineering, Technology & Applied Science Research*, 3(6):562-565.
- 471 2. Ardebili ZA, Gabr MA, Rahman MS (2016). Uplift Capacity of Plate Anchors in
472 Saturated Clays: Analyses with Different Constitutive Models. *International*
473 *Journal of Geomechanics*, 16(2), 4015053.
- 474 3. Bhattacharya, P., and Kumar, J. (2014). Vertical pullout capacity of horizontal
475 anchor plates in the presence of seismic and seepage forces. *Geomechanics*
476 *and Geoengineering*, 9(4):294-302.
- 477 4. Bolton, M. D. (1986). The strength and dilatancy of sands. *Géotechnique*
478 36(1):65-78
- 479 5. Brinkgreve, R.B.J., and Vermeer, P.A. (2001). Plaxis Finite Element Code for
480 Soil and Rock Analyses, Version 1, BALKEMA.
- 481 6. Clemence SP, Veesaert CJ (1977) Dynamic pullout resistance of anchors in
482 sand. In: roceedings of the International Symposium on Soil-Structure
483 Interaction, Roorkee, India, pp 389–397
- 484 7. Das B. M., Yang Jin-Kaun (1987), Uplift Capacity of Model Group Anchors in
485 Sand. Foundations for Transmission Line Towers, *Geotechnical Special*
486 *Publication* No. 8, ASCE
- 487 8. Das, B. M. (1978). Model tests for uplift capacity of foundations in clay. *Soils*
488 *and Found.* 18(2):17-24.
- 489 9. Das, B.M., (1983). A procedure for estimation of uplift capacity of rough piles.
490 *Soils and Found.*, Japan, 23(3):122-126.
- 491 10. Das, B. M. (1990). *Earth Anchors. Developments in Geotechnical Engineering*,
492 50: 1-241.

- 493 11. Emirler, B. Bildik, S., and Laman, M. (2015). Numerical Investigation of Group
494 Anchors. *IFCEE 2015* © ASCE 279–288.
- 495 12. Ganesh, R., and Sahoo, J. P. (2015). Influence of ground water on the
496 ultimate uplift resistance of circular plate anchors. *50th Indian geotechnical*
497 *Conference 17th - 19th December 2015, Pune, Maharashtra, India.*
- 498 13. Geddes, J.D., and Murray, E.J. (1996). Plate anchor groups pulled vertically in
499 sand. *J. Geotech. Engrg.*, ASCE 122(7):509–516.
- 500 14. Ghosh, P., and Kumari, R. (2012) Seismic interference of two nearby
501 horizontal strip anchors in layered soil. *Nat Hazards*, 63:789–804
- 502 15. Hanna, A., Ayadat, T., and Sabry, M. (2007). Pullout resistance of single
503 vertical shallow helical and plate anchors in sand. *Geotechnical and*
504 *Geological Engineering*, 25(5):559–573.
- 505 16. Hanna A, Rahman F, Ayadat T (2011) Passive earth pressure on embedded
506 vertical plate anchors in sand. *Acta Geotechnica*, 6(1), 21–29.
- 507 17. Ilamparuthi, K., Dickin, E. A., and Muthukrisnaiah, K. (2002). Experimental
508 investigation of the uplift behaviour of circular plate anchors embedded in
509 sand. *Can. Geotech. J.*, 39: 648–664.
- 510 18. Khatri, V. N., and Kumar, J. (2009). Vertical uplift resistance of circular plate
511 anchors in clays under undrained condition. *Computers and Geotechnics*,
512 36(8):1352–1359.
- 513 19. Khatri, V. N., and Kumar, J. (2010). Stability of an unsupported vertical circular
514 excavation in clays under undrained condition. *Computers and Geotechnics*,
515 37(3):419–424.
- 516 20. Khatri, V. N., and Kumar, J. (2011). Effect of anchor width on pullout capacity
517 of strip anchors in sand. *Canadian Geotechnical Journal*, 48(3):511–517.

- 518 21. Kouzer, K. M., and Kumar, J. (2009a). Vertical uplift capacity of two interfering
519 horizontal anchors in sand using an upper bound limit analysis. *Computers*
520 *and Geotechnics*, 36(6):1084–1089.
- 521 22. Kouzer, K. M., and Kumar, J. (2009b). Vertical uplift capacity of equally
522 spaced horizontal strip anchors in sand. *International Journal of*
523 *Geomechanics*, 9(5):230-236.
- 524 23. Kumar, J., and Kouzer, K.M. (2008a). Vertical uplift capacity of a group of
525 shallow horizontal anchors in sand. *Géotechnique*, 58(10):821–823.
- 526 24. Kumar, J., and Naskar, T. (2012). Vertical uplift capacity of a group of two
527 coaxial anchors in a general $c-\phi$ soil. *Canadian Geotechnical Journal*, 49(3):
528 367–373.
- 529 25. Mabrouki, A., and Mellas, M. (2014). Étude tridimensionnelle de la capacité
530 ultime des plaques d'ancrage dans un sol frottant. *Courrier Du Savoir*,
531 (18):15–19.
- 532 26. Merifield, R.S., and Sloan, S.W. (2006). The ultimate pullout capacity of
533 anchors in frictional soils. *Can. Geotech. J.* 43(8):852–868.
- 534 27. Merifield R S, Lyamin A V, Sloan S W (2006) Three dimensional lower bound
535 solutions for the stability of plate anchors in sand. *Géotechnique* 56(2):123–
536 132.
- 537 28. Merifield, R.S and Smith, C.C. (2010). The ultimate uplift capacity of multi-
538 plate strip anchors in undrained clay. *Computers and Geotechnics* 37:504–514
- 539 29. Meyerhof, G. G. and Adams, J. I. (1968). The ultimate uplift capacity of
540 foundations. *Canadian Geotechnical Journal* 5(4):225–244.
- 541 30. Meyerhof, G. G. (1973) “Uplift resistance of inclined anchors and piles” Proc.
542 of VIII International Conference on Soil mechanics and Foundation
543 Engineering, Moscow, USSR, 2, 1, 167-172.

- 544 31. Mors, H. (1959). The behaviour of mast foundations subject to tensile forces.
 545 *Bautechnik*, 10: 367–378.
- 546 32. Murray, E. J., and Geddes, J. D. (1987). Uplift of anchor plates in sand. *J.*
 547 *Geotech. Engrg.*, 113(3):202–215.
- 548 33. Rowe, R. K. and Davis, E. H. (1982b). The behaviour of anchor plates in sand.
 549 *Géotechnique*, 32(1):25–41.
- 550 34. Sahoo, J. P., and Kumar, J. (2014a). Vertical uplift resistance of two closely
 551 spaced horizontal strip anchors embedded in cohesive – frictional weightless
 552 medium. *Can. Geotech. J.*, 51:223–230.
- 553 35. Sahoo, J. P., and Kumar, J. (2014b). Vertical uplift resistance of two interfering
 554 horizontal anchors in clay. *J. Geotech. Geoenviron. Eng.*, 140(4):06013007
- 555 36. Wang, D., Merifield, R.S., and Gaudin, C. (2013). Uplift behaviour of helical
 556 anchors in clay. *Can. Geotech. J.* 50:575-584.

557

558 **Appendix A: Analytical solution of break-out factor $N_{\gamma \text{ isolated}}$ for an isolated**
 559 **square anchor plate**

560 Volumes of the portions 1, 2 and 3 shown in Fig. 25:

$$V_1 = B^2H \quad (21)$$

$$V_2 = 0.5BH^2 \tan \theta \quad (22)$$

$$V_3 = \frac{1}{6}H^3 \tan^2 \theta \quad (23)$$

561 The ultimate pullout load Q_u is equal to the weight of the soil located within the failure
 562 mechanism:

$$Q_u = \gamma(V_1 + 4V_2 + 4V_3) \quad (24)$$

563 Using Equations 21, 22 and 23, we finally get:

$$Q_u = B^2\gamma H + 2\gamma H^2 B \tan \theta + \frac{2}{3}\gamma H^3 \tan^2 \theta \quad (25)$$

564 By definition, the ultimate pullout capacity q_u :

$$q_u = \frac{Q_u}{A} = \frac{Q_u}{B^2} \quad (26)$$

$$q_u = \gamma H \left(1 + 2 \frac{H}{B} \tan \theta + \frac{2}{3} \left(\frac{H}{B} \right)^2 \tan^2 \theta \right) \quad (27)$$

565 By convention, q_u is also given by:

$$q_u = \gamma H N_\gamma \quad (28)$$

566 So that the break-out factor N_γ for an isolated square plate anchor is:

$$N_{\gamma \text{ isolated}} = 1 + 2 \frac{H}{B} \tan \theta + \frac{2}{3} \left(\frac{H}{B} \right)^2 \tan^2 \theta \quad (29)$$

567 **Appendix B: Analytical solution of break-out factor $N_{\gamma \text{ end}}$ for a square anchor**
568 **plate located at an end**

569 For two or n square anchor plates with $S < 2H \tan \theta$, the ultimate pullout load of one
570 anchor plate at the end is equal to the weight of the soil located within its failure
571 mechanism defined by points a, b, c, d, e shown in Fig. 21.

572 Volumes of the portions 4 and 5 shown in Fig. 26:

$$V_4 = \frac{1}{2}(2H \tan \theta - S) \left(H - \frac{S}{2} \cot \theta \right) B \quad (30)$$

$$V_4 = BH^2 \tan \theta + B \frac{S^2}{4} \cot \theta - BSH \quad (31)$$

$$V_5 = \frac{1}{3} \times \frac{1}{2} \left(\sqrt{2}H \tan \theta - S \frac{\sqrt{2}}{2} \right)^2 \left(H - \frac{S}{2} \cot \theta \right) \quad (32)$$

$$V_5 = \frac{1}{3} H^3 \tan^2 \theta - \frac{1}{2} SH^2 \tan \theta - \frac{S^3}{24} \cot \theta + \frac{1}{4} S^2 H \quad (33)$$

573 The volume V corresponding to points a, b, c, d, e shown in Fig.16 is equal to:

$$V = V_T - \frac{1}{2} V_4 - 2 \left(\frac{1}{2} V_5 \right) = V_T - \frac{V_1}{2} - V_5 \quad (34)$$

574 Where V_T is the total volume of soil located within the failure mechanism for an
 575 isolated square anchor plate.

576 So:

$$V = B^2H + \frac{3}{2}H^2B \tan \theta + \frac{1}{3}H^3 \tan^2 \theta - \frac{1}{8}BS^2 \cot \theta + \frac{1}{2}BSH + \frac{1}{2}SH^2 \tan \theta + \frac{1}{24}S^3 \cot \theta - \frac{1}{4}S^2H \quad (35)$$

577 The ultimate pullout capacity of anchor plate located at the end is then:

$$q_{u \text{ end}} = \frac{Q_{u \text{ end}}}{A} = \frac{Q_{u \text{ end}}}{B^2} = \frac{\gamma \times V}{B^2} \quad (36)$$

578 Using Equation 35, we get:

$$q_{u \text{ end}} = \gamma H \left(1 + \frac{3}{2} \left(\frac{H}{B} \right) \tan \theta + \frac{1}{3} \left(\frac{H}{B} \right)^2 (\tan \theta)^2 - \frac{1}{8} \left(\frac{S}{B} \right) \left(\frac{S}{H} \right) \cot \theta + \frac{1}{2} \left(\frac{S}{B} \right) + \frac{1}{2} \left(\frac{S}{B} \right) \left(\frac{H}{B} \right) \tan \theta + \frac{1}{24} \left(\frac{S}{B} \right)^2 \left(\frac{S}{H} \right) \cot \theta - \frac{1}{4} \left(\frac{S}{B} \right)^2 \right) \quad (37)$$

579 Since:

$$q_{u \text{ end}} = \gamma H N_{\gamma \text{ end}} \quad (38)$$

580 We finally obtained $N_{\gamma \text{ end}}$

$$N_{\gamma \text{ end}} = 1 + \frac{1}{3} \left(\frac{H}{B} \right)^2 (\tan \theta)^2 + \frac{1}{2} \left(3 + \frac{S}{B} \right) \frac{H}{B} \tan \theta + \frac{1}{8} \frac{S}{H} \frac{S}{B} \left(\frac{1}{3} \frac{S}{B} - 1 \right) \cot \theta - \frac{1}{4} \left(\frac{S}{B} \right)^2 + \frac{1}{2} \frac{S}{B} \quad (39)$$

581

582 **Appendix C: Analytical solution of break-out factor $N_{\gamma \text{ inter}}$ for an intermediate**
 583 **square anchor plate**

584 For n square anchor plates in row configuration with $S < 2H \tan \theta$, the ultimate pullout
 585 load of an intermediate anchor plate is equal to the weight of the soil located within
 586 its failure mechanism defined by points a, b, c, d, e, f as shown in Fig. 23. The break-
 587 out factor corresponding to this volume is noted $N_{\gamma \text{ inter}}$

588 The volume V corresponds to points a, b, c, d, e, f shown in Fig.18 is equal to:

$$V = V_T - 2 \left(\frac{1}{2} V_4 \right) - 4 \left(\frac{1}{2} V_5 \right) = V_T - V_4 - 2V_5 \quad (40)$$

589 Where V_T is the total volume of soil located within the failure mechanism for an
590 isolated square anchor plate.

591 Using Equations (31 and 33), we obtain:

$$V = B^2 H + H^2 B \tan \theta - \frac{1}{4} B S^2 \cot \theta + B S H - S H^2 \tan \theta + \frac{1}{12} S^3 \cot \theta - \frac{1}{2} S^2 H \quad (41)$$

592 The ultimate pullout capacity of one anchor plate located between two anchor plates
593 is given by:

$$q_{u \text{ inter}} = \frac{Q_{u \text{ inter}}}{A} = \frac{Q_{u \text{ inter}}}{B^2} = \frac{\gamma \times V}{B^2} \quad (42)$$

$$q_{u \text{ inter}} = \gamma H \left(1 + \left(\frac{H}{B} \right) \tan \theta - \frac{1}{4} \left(\frac{S}{B} \right) \left(\frac{S}{H} \right) \cot \theta + \frac{S}{B} + \left(\frac{S}{B} \right) \left(\frac{H}{B} \right) \tan \theta \right. \\ \left. + \frac{1}{12} \left(\frac{S}{B} \right)^2 \left(\frac{S}{H} \right) \cot \theta - \frac{1}{2} \left(\frac{S}{B} \right)^2 \right) \quad (43)$$

594 Since:

$$q_{u \text{ inter}} = \gamma H N_{\gamma \text{ inter}} \quad (44)$$

595 We get:

$$N_{\gamma \text{ inter}} = 1 + \left(1 + \frac{S}{B} \right) \frac{H}{B} \tan \theta - \frac{1}{3} \frac{S}{B} \frac{S}{H} \left(\frac{1}{4} \frac{S}{B} - 1 \right) \cot \theta - \frac{1}{2} \left(\frac{S}{B} \right)^2 + \frac{S}{B} \quad (45)$$

596

597 List of figures captions:

598 Fig. 1 Geometrical model of group of four square anchor plates

599 Fig. 2 Total displacements for an isolated square anchor plate ($H/B=4$)

600 Fig. 3 Influence of Young's modulus on the pullout load for an isolated plate ($H/B = 4,$

601 $H/B = 6$)

602 Fig. 4 Group of square anchor plates in row configuration

603 Fig. 5 The ultimate pullout load versus displacement for two anchor plates with

604 varying spacing and an isolated anchor plate

605 Fig. 6 Deformed mesh for two anchor plates, $H/B = 2$ and $S/B = 2$

606 Fig. 7 Group efficiency of square anchor plates in row configuration

607 Fig. 8 Group of square anchor plates in square configuration

608 Fig. 9 Total displacements for nine (3 x 3) anchor plates in square configuration, H/B

609 $= 4$ and $S/B = 2$

610 Fig. 10 Group efficiency for four and nine plates in square configuration

611 Fig. 11 Load factor of group of square plates in row configuration

612 Fig. 12 Load factor of group of square plates in square configuration

613 Fig. 13 Influence of installation depth on the group efficiency

614 Fig. 14 Total displacements for a group of two plates with $H/B = 4 ; 6 ; 8$ and 10

615 Fig. 15 Influence of internal friction angle of soil on the group efficiency

616 Fig. 16 Influence of dilation angle on the group efficiency

617 Fig. 17 Influence of anchor roughness on the group efficiency

618 Fig. 18 Modified failure mechanism

619 Fig. 19 Break-out factor for square anchor plate in cohesionless soil

620 Fig. 20 Comparison of analytical and numerical Break-out factor for square anchor

621 plate ($B=1\text{m}$) in cohesionless soil

622 Fig. 21 Interference of two anchor plates: (a) 3D view, (b) Cross section A-A'

623 Fig. 22 Numerical, analytical and experimental comparison of group efficiency of two

624 square anchor plates

625 Fig. 23 Interference of n square anchor plates: (a) 3D view, (b) Cross section A-A'

626 Fig. 24 Comparison of numerical, analytical and experimental results of group

627 efficiency of five square plates in row configuration

628 Fig. 25 Failure mechanism for isolated square plate

629 Fig. 26 Interference detail of two failure mechanisms

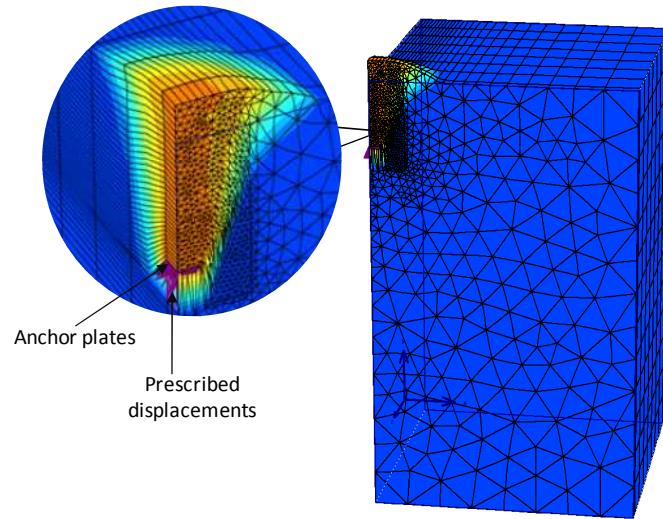


Fig. 2

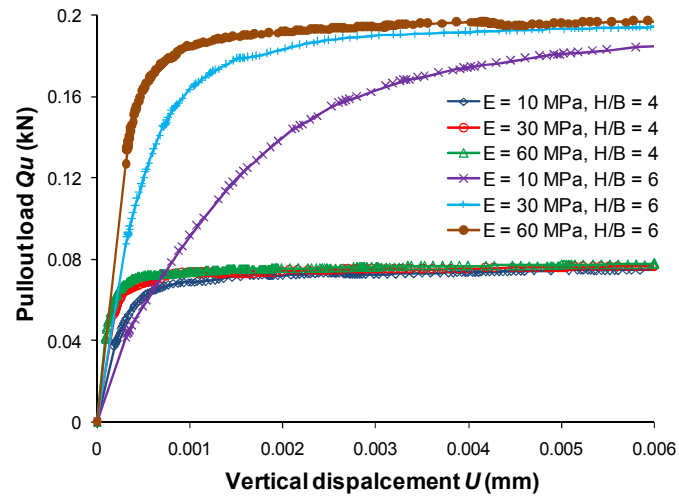


Fig. 3

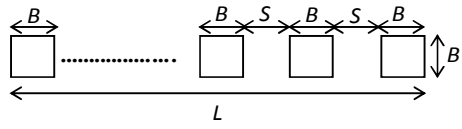


Fig. 4

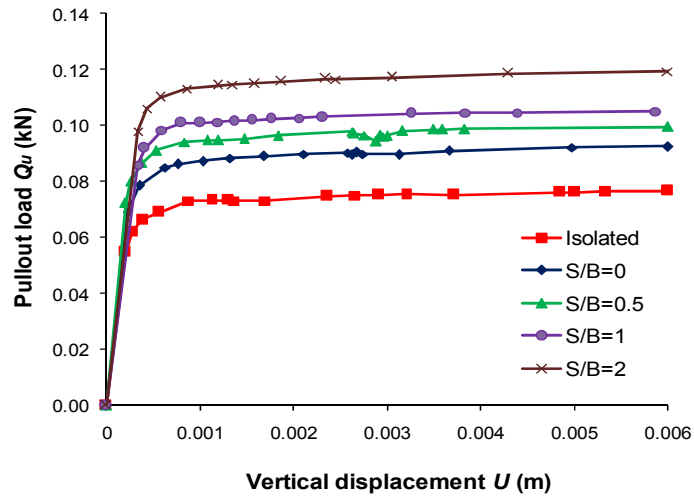


Fig. 5

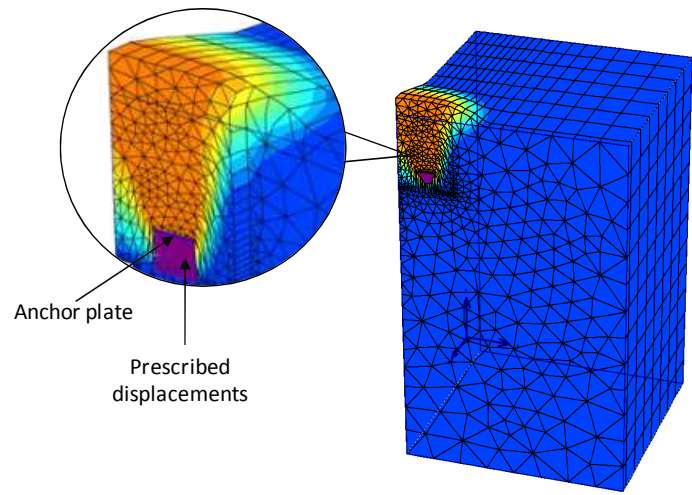


Fig. 6

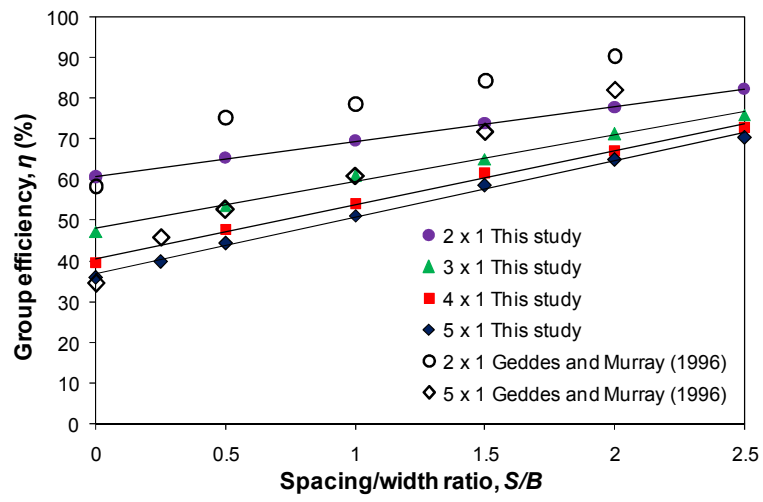


Fig. 7

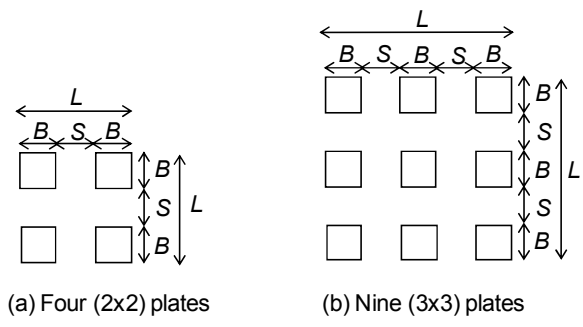


Fig. 8

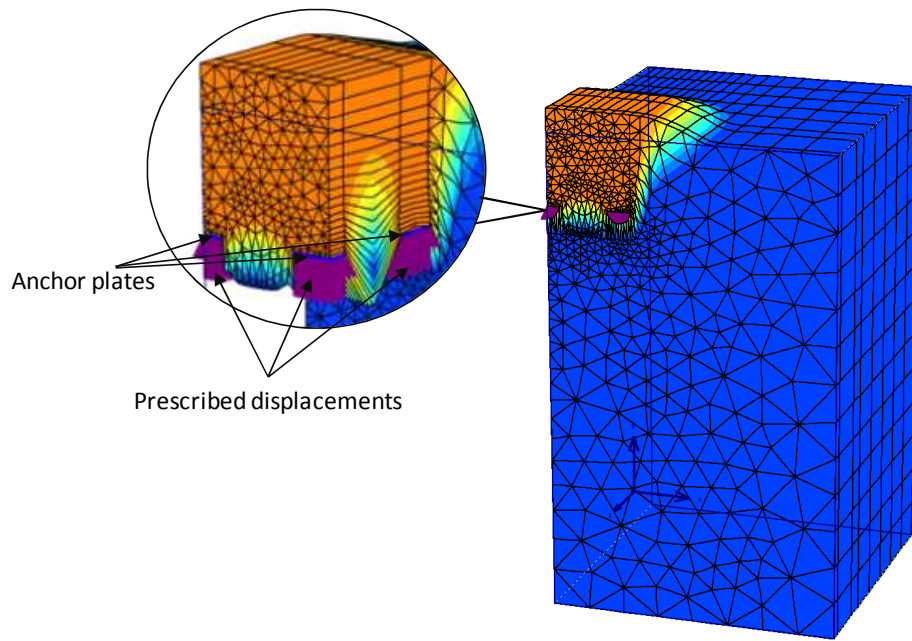


Fig. 9

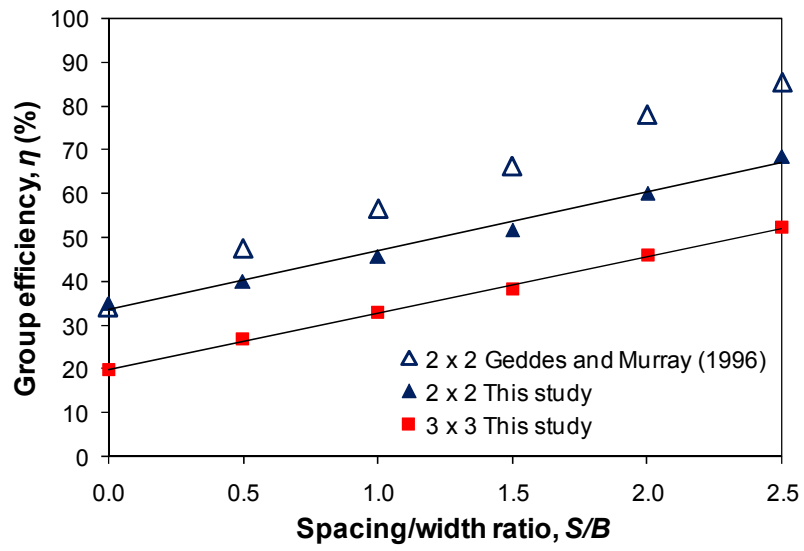


Fig. 10

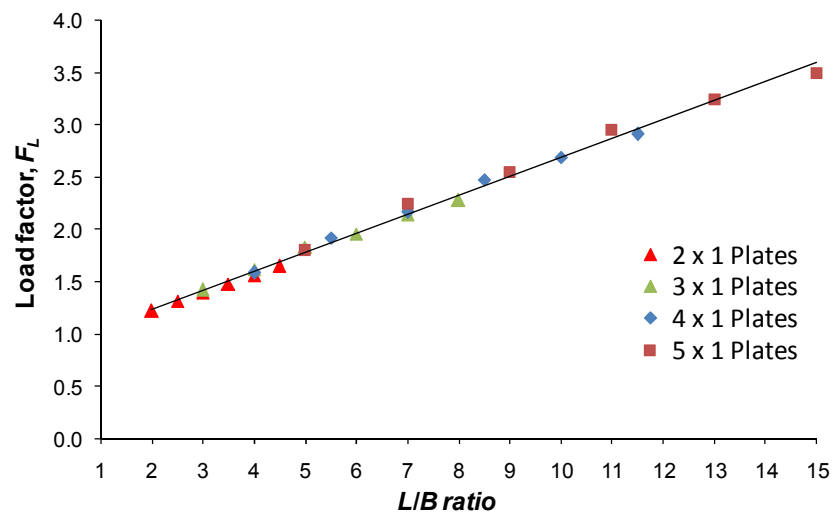


Fig. 11

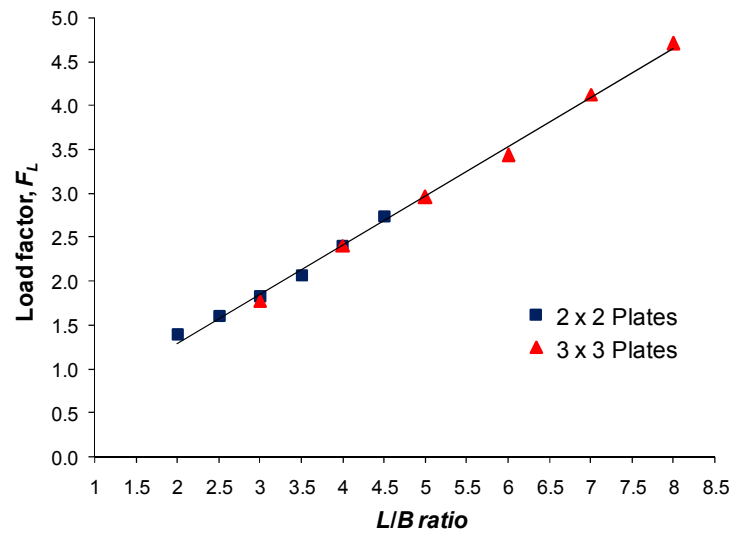


Fig. 12

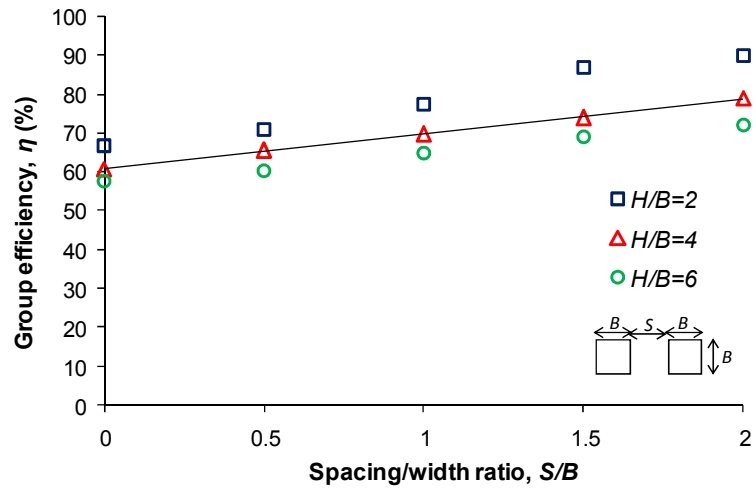


Fig. 13

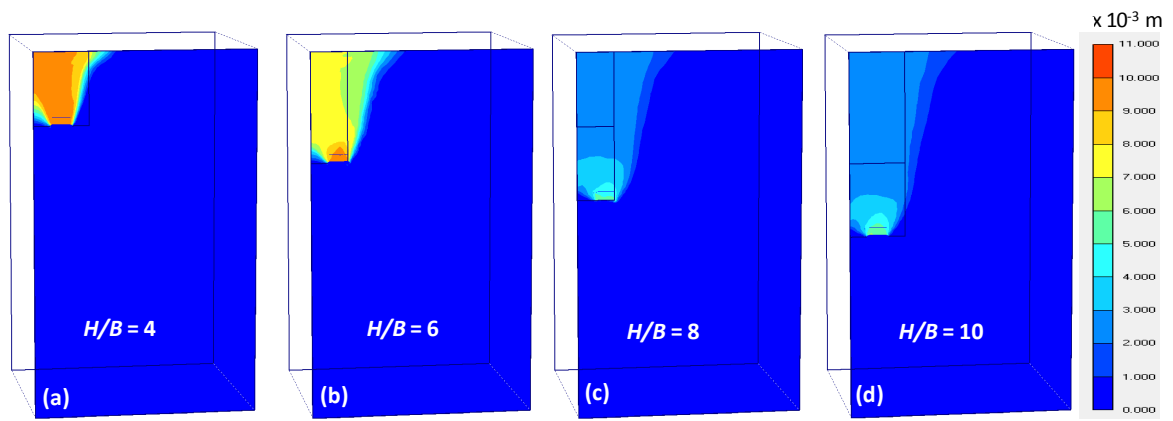


Fig. 14

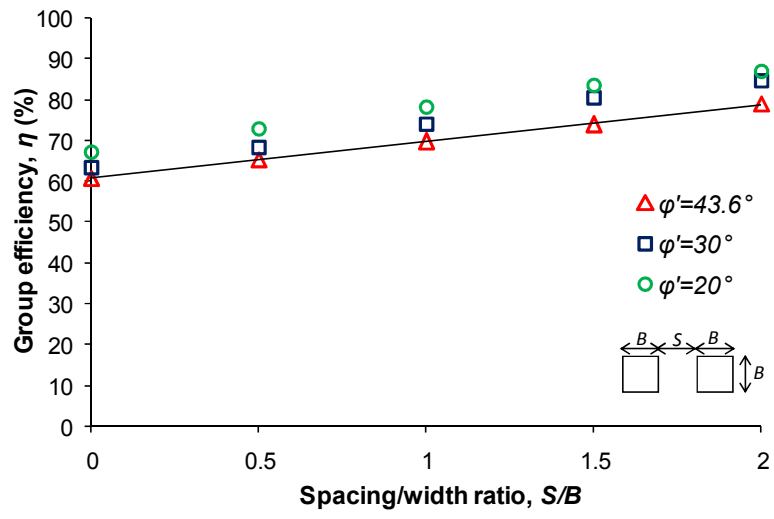


Fig. 15

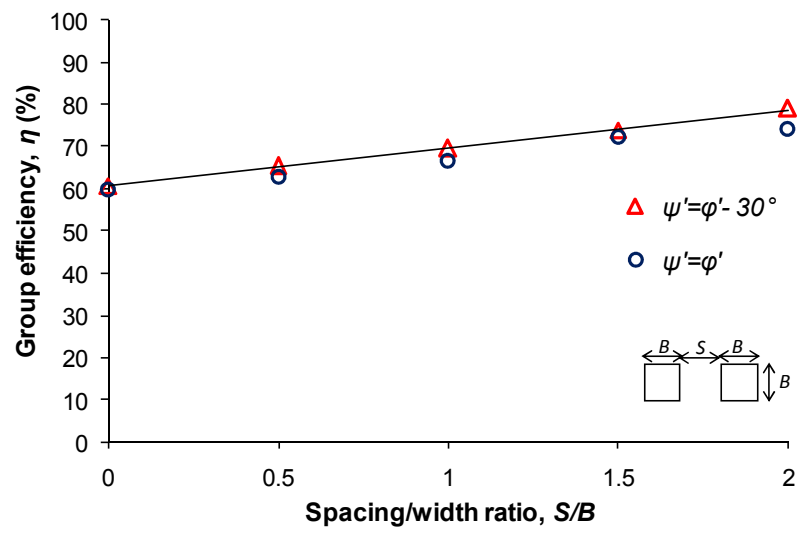


Fig. 16

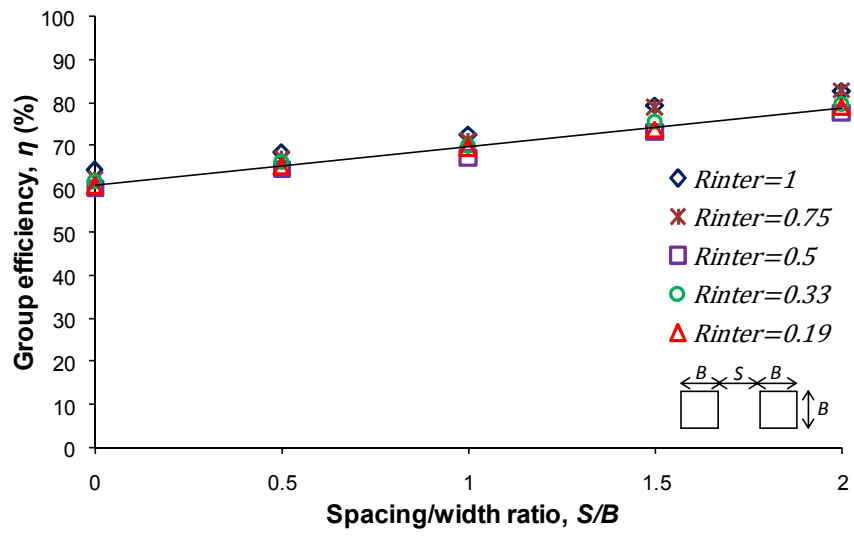


Fig. 17

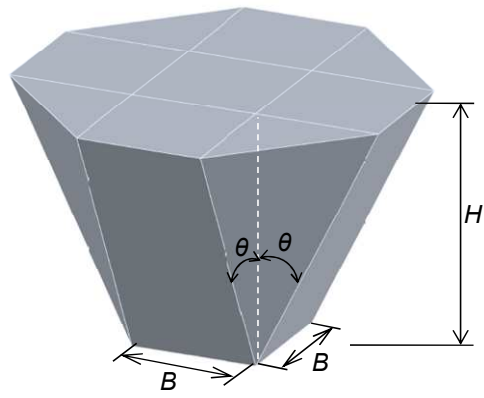


Fig. 18

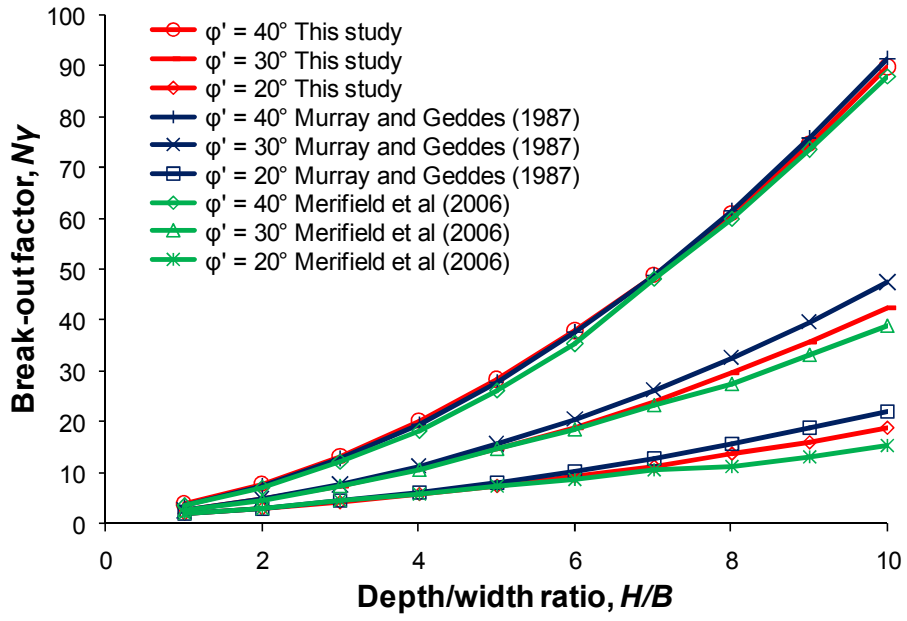


Fig. 19

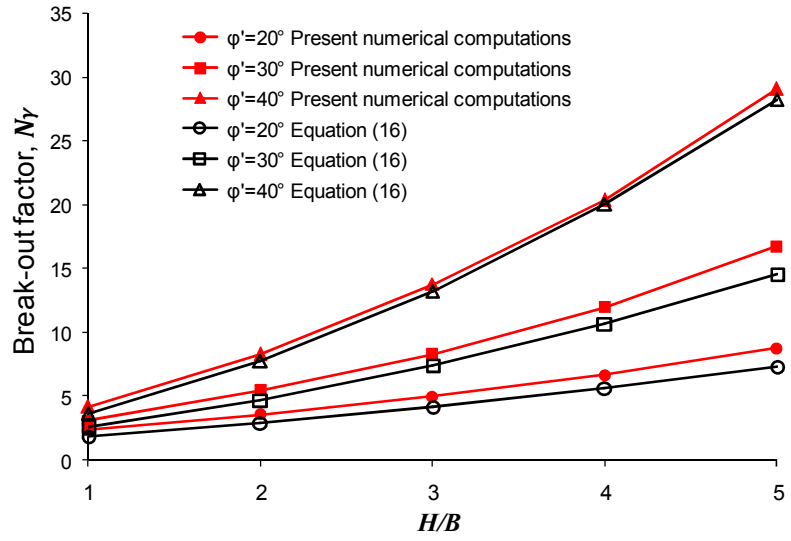


Fig. 20

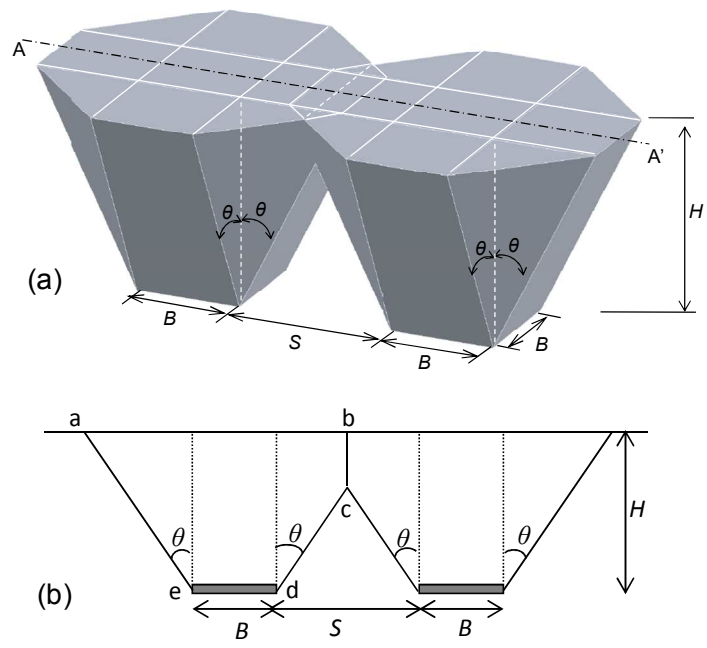


Fig. 21

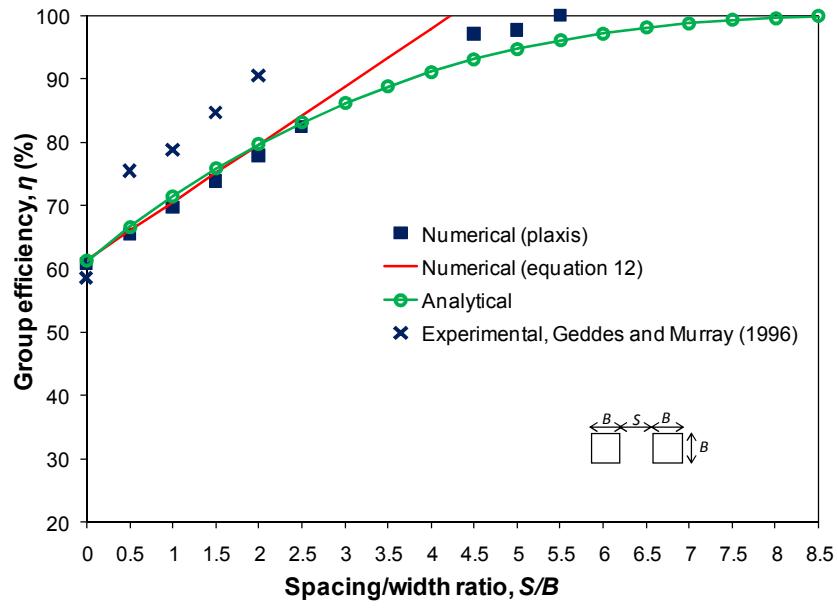


Fig. 22

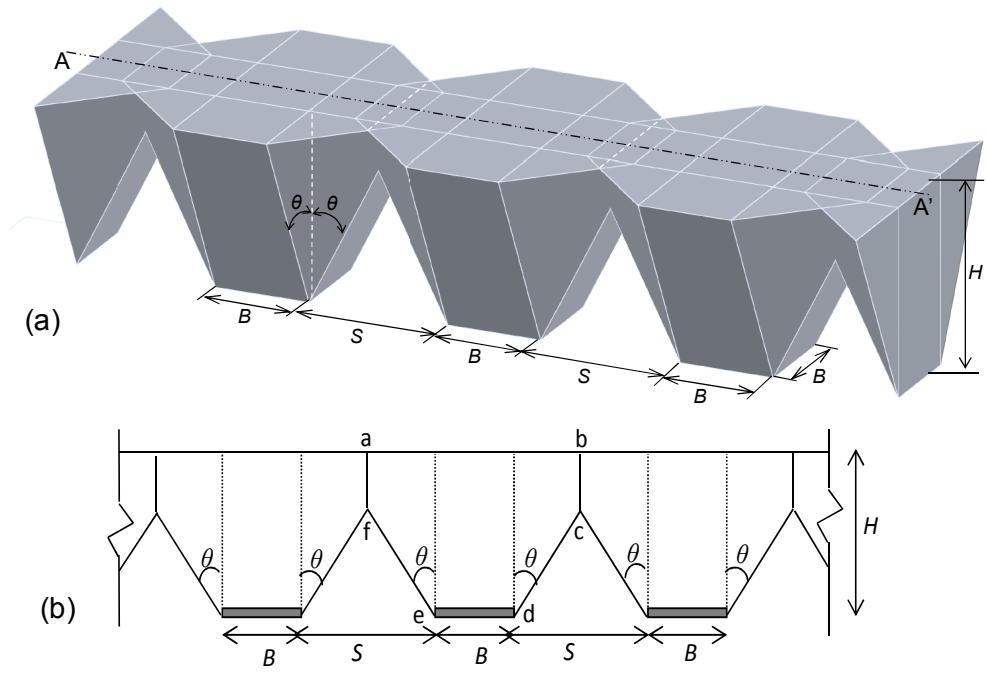


Fig. 23

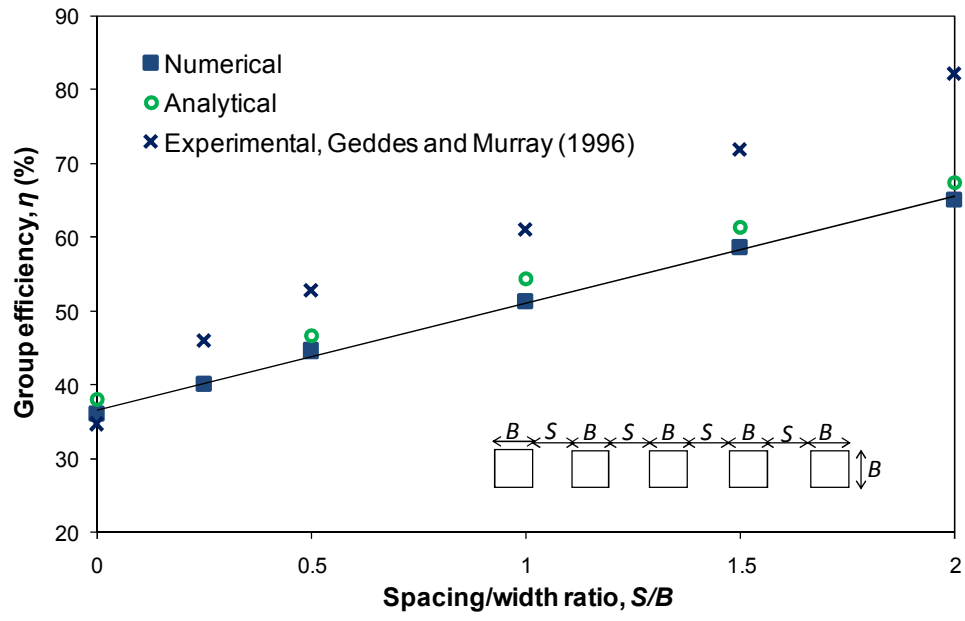


Fig. 24

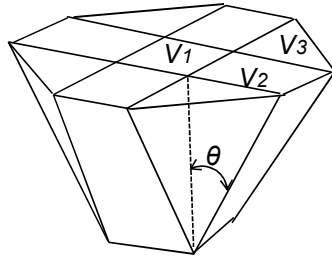


Fig. 25

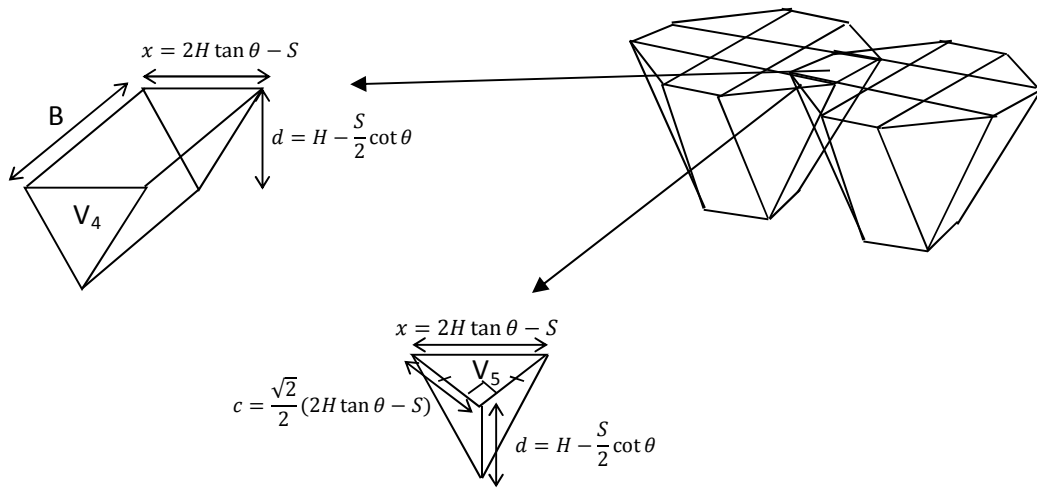


Fig. 26